Colloids and Surfaces A: Physicochemical and Engineering Aspects 714 (2025) 136541

Contents lists available at ScienceDirect

Colloids and Surfaces A: Physicochemical and Engineering Aspects

journal homepage: www.elsevier.com/locate/colsurfa

High-throughput millifluidics for monodisperse alginate milli-capsules filled with emulsions

Johannes Marburger [a], Goran T. Vladisavljević [b], Nico Leister [a,*]

[a] Institute of Process Engineering in Life Sciences, Chair of Food Process Engineering, Karlsruhe Institute of Technology, Karlsruhe, Germany
[b] Department of Chemical Engineering, Loughborough University, Loughborough LE11 3TU, United Kingdom

HIGHLIGHTS

- Emulsion-alginate core-shell capsules were produced by capillary co-extrusion.
- Precise capillary alignment was achieved using CNC milled Lego-inspired holder.
- Encapsulation efficiency of w/o emulsion was 90–100 %.
- Monodispersed capsules were produced at throughput of up to 240 ml/h.
- Emulsion loading reached 73 % at optimized flow rate ratio.

GRAPHICAL ABSTRACT

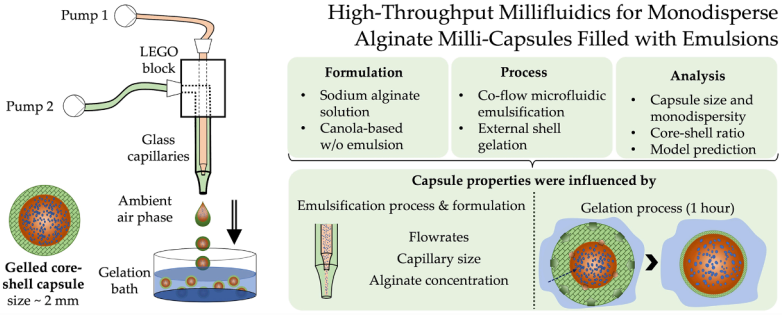

ARTICLE INFO

Keywords:
Millifluidics
Alginate hydrogel
Emulsion
Core-shell capsule
Particle
Dripping-to-jetting transition
Co-flow

ABSTRACT

Structured multiphase capsules based on biopolymers promise broad applications in life science related research and industry. For making these complex structures with high accuracy, various microfluidic emulsification techniques were used. However, the limited throughput of these methods remains a challenge. Within this study, millimetre-sized core-shell capsules, consisting of a liquid water-in-oil emulsion core surrounded by a gelled alginate shell, were produced by co-extrusion of two immiscible phases through coaxial capillaries. The inner capillary tip was placed upstream of the outer capillary tip which allowed high production throughputs. Droplet generation in a quiescent ambient air followed by external shell gelation yielded large, monodisperse capsules of around 2 mm in diameter with the capsule filling degree above 70 % and the encapsulation efficiency of 90–100 %. The throughput, capsule size, and dripping dynamics were controlled by the orifice size of outer capillary, fluid flow rates and alginate concentration. The critical Weber number and the breakup lengths of compound jet were significantly affected by the viscosity of alginate solution. The total flowrate in dripping regime was up to 240 ml/h using 1 wt% alginate solution and the coefficient of variation of capsule sizes was less than 5 %. Further experiments elucidated the influence of the gelation step on the shell and core volume. The developed model predicted the final capsule size and the loading capacity of capsules with an accuracy above 97 %. The findings of this study confirm the ability of in-air millifluidics to generate complex structured particles with precisely controlled attributes at high throughputs.

* Corresponding author.
E-mail address: nico.leister@kit.edu (N. Leister).

https://doi.org/10.1016/j.colsurfa.2025.136541
Received 8 January 2025; Received in revised form 12 February 2025; Accepted 27 February 2025
Available online 1 March 2025
0927-7757/© 2025 The Author(s). Published by Elsevier B.V. This is an open access article under the CC BY license (http://creativecommons.org/licenses/by/4.0/).

1. Introduction

Core-shell capsules offer a wide range of applications due to their compartmentalized structure and advantages compared to matrix-type capsules, such as high loading capacity of liquid payloads, better protection of cargos against evaporation or degradation, and a burst release of core material when the capsules are broken, which allows rapid release of actives, such as flavor in chewing gum [1] or fragrance in scratch and sniff stickers [2]. Core-shell capsules usually consist of a solid or semisolid shell and a liquid core, which allows for unique combinations of textures and properties of both materials. This structure makes these capsules highly desirable as microreactors, controlled release vehicles, and 3D microenvironments for the growth of microorganisms and cells [3]. Depending on the application, different core and shell materials are chosen.

Alginate is a readily available natural polymer widely used in life sciences and engineering, due to its biocompatibility and the ability to form hydrogels by ionotropic gelation [4]. It is an approved food additive and widely used in the food industry as a thickener, stabilizer, and gelling agent [5]. The internal liquid phase of alginate core-shell capsules is usually immiscible with alginate solution to maintain a sharp interface between the two liquid phases during the production process and create a core-shell morphology after gelling. Therefore, vegetable oils or water-in-oil (w/o) emulsions are obvious choices for the core liquid in food applications. The incorporation of dispersed water phase in the encapsulated oily core reduces the total fat content and enables additional functional properties such as double encapsulation of water-soluble ingredients and their extended or delayed release [6,7], as well as masking the taste of functional nutrients of unpleasant flavour [8–11].

The capsules, which consist of a gelled, water-based alginate shell and a liquid, oil-based emulsion core, promise applications in various fields [12] including biotechnology [3], pharmaceutics [13], cosmetics [14], and food industry [15]. The production of such a complex multiphase product containing three phases in two aggregate states remains a significant challenge, especially when additional quality attributes of these products are needed, like a high size uniformity, spherical shape, a controllable loading capacity and shell thickness, or a relatively large size in millimetre range, e.g., in food or pharmaceutical industry [16].

Classical emulsification processes, which rely on the top-down principle, are widely used in industry due to reliability, good process stability over time and high throughputs. However, they often fail to produce multiple emulsions with the required quality attributes and high encapsulation efficiency due to high shear stresses exerted on the droplets [17]. Alternative bottom-up emulsification techniques like membrane emulsification and droplet microfluidics can overcome these challenges. Additionally, they offer high energy efficiency, mild process conditions [18], and can generate multiphase emulsions with an extraordinary precision [19]. Alginate core-shell capsules were produced in microfluidic devices using internal gelation, external gelation, and inverse gelation mechanisms to harden the shell liquid [6,14]. The main production challenge in the reported studies was limited throughput, often just several millilitres per hour [6,20,21], which impedes the wider adoption of microfluidic technology. Thus, it remains a challenge to produce large, monodisperse, and spherical core-shell capsules with a competitive throughput using microfluidics. It is because an increased throughput often results in decreased product quality with less monodisperse and spherical particles [3,22,23].

In this work, a novel millifluidic approach was developed to fabricate milli-capsules composed of a gelled alginate shell filled with a liquid w/o emulsion. The method involves the co-extrusion of core and shell liquid streams through coaxial tapered-end glass capillaries. The inner capillary tip was placed upstream of the outer capillary tip which reduced shear stresses between the inner and outer stress before exiting the outer capillary. Core-shell drops were generated in a quiescent ambient air which resulted in larger capsules compared to chip-based microfluidic systems where core/shell droplets are formed in another liquid stream. The aim was to produce alginate core-shell capsules with a relatively large diameter of 1.5–2.5 mm at high throughput (above 200 ml/h). The experimental procedure was divided in three steps depicted in Fig. 1.

First, different materials were evaluated based on their suitability to form stable core-shell capsules. Secondly, a co-flow extrusion system was selected, for the advantages of good process control, high process stability over time and reduced start-up times [24]. Thirdly, swelling or shrinking of different regions the capsules was evaluated following their storage in a gelation bath.

Based on the results of other works, it is known that co-extrusion process is capable of producing stable capsules with a gelled alginate shell and a liquid w/o emulsion core at low throughput [7]. A quiescent ambient air should ensure that droplets are generated by gravity-assisted dripping, which is expected to form large, spherical and monodisperse capsules [6,21]. At low flowrates, the droplet size is a function of the orifice size and surface tension [25,26]. An increase of the flowrates should lead to inertial forces to become more dominant, which will eventually cause the transition from dripping to jetting and the formation of smaller and polydisperse capsules [22,23]. This work identifies process windows in the transitional region between dripping and jetting in which highly uniform droplets are produced at relatively high flow rates. The flow rates in this study were up to 10 times higher than in similar studies [7]. By combining the break-up points of the inner droplet and the outer droplet into single break-up point, the filling degree and the capsule size could be adjusted more independently without an additional dilution.

Alginate concentration significantly affects the solution viscosity and surface tension and the resulting change in the dripping dynamics is expected to influence capsule properties, like size and sphericity [27]. Since the physical properties of fluids play a key role in droplet generation and capsule properties they were measured and added to calculations. The process was investigated using dimensionless numbers and the corresponding scaling laws.

The filling degree of capsules (the percentage of the capsule volume occupied by liquid core) was maximised by increasing the flow rate ratio of inner to outer phase up to the critical value, when the shell became too thin and ruptured upon jet breakup or during gelation. In addition, the filling degree of the capsules was found to be a dynamic property and varied during storage, due to shrinkage and swelling processes. One of the objectives of this study was to develop a model equation with empirical fitting constants to predict the filling degree of capsules based on flow rate ratio, alginate concentration, and storage conditions.

2. Methods

2.1. Solutions

To prepare aqueous alginate solutions, alginic acid sodium salt (Carl Roth GmbH + Co. KG, Karlsruhe, Germany) was dissolved in deionized water at 40 °C. The solution was homogenized with an Ultra-Turrax® system, UT, (Ultra-Turrax T25, IKA, Germany) at 12,000 rpm (tip speed 8.16 ms^{-1}) for at least 3 min. Solutions were stored for at least one day at 5 °C to ensure disappearance of gas bubbles and complete unfolding of polymer chains. The gelling solution was 0.34 M (2 wt%) $CaCl_2$ prepared by dissolving anhydrous $CaCl_2$ powder (Sigma-Aldrich, Saint Louis, MO, USA) in deionized water.

To prepare the continuous phase of w/o emulsions, 1 wt% polyglycerol polyricinoleate (PGPR, Palsgaard, Juelsminde, Denmark) was dissolved in canola oil (Mystic Moments, Fordingbridge, United Kingdom, density = 914 g/l). The dispersed water phase was 0.34 M $CaCl_2$ solution. Emulsions with a dispersed phase content of 30 wt% were prepared in two steps using the UT system: 15 g of water phase was slowly added to 35 g of oil phase under constant stirring at 5000 rpm (tip speed 3.4 ms^{-1}), followed by homogenization for 1 min at 24,000 rpm (tip speed 16.3 ms^{-1}). All emulsions were stored at

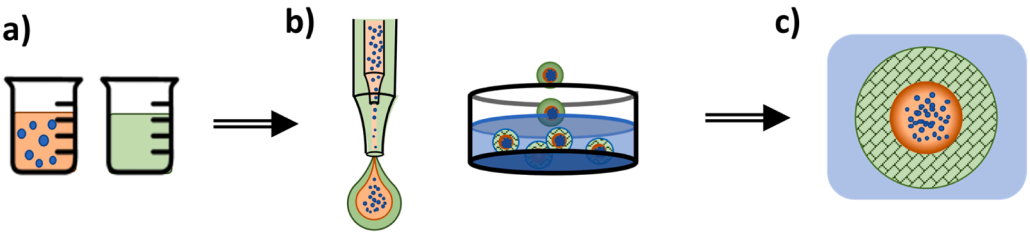

Fig. 1. Experimental steps in this study: a) Selection of materials (w/o emulsion and alginate solution) for core-shell droplet generation; b) Optimisation of droplet generation and shell jellification; c) Investigation of swelling/shrinking of capsules during storage in a gelation bath.

Table 1
Surface tension and viscosity (average and standard deviation of triplicates) of used alginate solutions.

Alginate concentration	1 wt%	2 wt%	3 wt%
Interfacial tension [mN/m]	52.6 ± 0.5	45.9 ± 0.9	38.7 ± 0.1
Viscosity at $\dot{\gamma} = 2.15\ s^{-1}$ [Pa s]	0.128 ± 0.008	0.917 ± 0.091	4.565 ± 0.492
Viscosity at $\dot{\gamma} = 215\ s^{-1}$ [Pa s]	0.089 ± 0.009	0.373 ± 0.046	1.217 ± 0.149

5 °C after preparation and used within 24 h.

Surface tension of alginate solutions in air was measured with the pendant drop method (OCA 15 LJ, DataPhysics Instruments GmbH, Germany), with 10 µl drop. Measurements were conducted for 20 min while collecting 30 data points per minute. All measurements were done in ambient air at 20 °C and executed in triplicate. Average interfacial tension values at quasi steady state (after 20 min) are listed in Table 1.

Dynamic viscosity of alginate solutions was measured with a Modular Compact Rheometer 301 (Anton Paar Group AG, Graz, Austria), using a double gap measuring system with a diameter of 26.66 mm (B-DG26.7). Measurements were done with $m = 4.5$ g sample, which was hold in the system for 1 min ($T = 25$ °C) before starting. The shear rate was increased logarithmically ($\dot{\gamma} = 1$–$1000\ s^{-1}$) while recording 19 data points, each separated by an interval of 15 s. Each sample was measured in triplicate by exchanging the used material. Average values of the measured viscosity at $\dot{\gamma} = 2.15\ s^{-1}$ and $\dot{\gamma} = 215\ s^{-1}$ are given in Table 1 and indicate a shear-thinning behaviour of alginate solutions for the typically applied shear rates in microfluidic devices.

2.2. Microfluidic process set-up and procedures

The experimental set-up is shown in Fig. 2a. The solutions were loaded into 10 ml or 20 ml plastic syringes and delivered by syringe pumps (LEGATO® 100, KD Scientific, Holliston, MA, USA). Volume flowrates of inner phase (Q_I) and outer phase (Q_O) were independently controlled, and the total volume flowrate (Q_T) was calculated as $Q_I + Q_O$. Teflon tubes were used to connect the syringes to the capillary holder [28]. The holder was made of polyoxymethylene and fabricated with a CNC milling machine (HAAS Automation, model Super Mini, Norwich, UK) based on 3D drawing created in SolidWorks® (Dassault Systems, Vélizy-Villacoublay, France). The holder enables the alignment of two capillaries and the distribution of both solutions from inlet tubes to the capillaries. All connections were tightly sealed with custom-made stainless-steel connectors and O-rings.

Borosilicate glass capillaries were acquired from World Precision Instruments (Friedberg, Germany) with the inner and outer diameters of 0.58 mm and 1.0 mm for the inner capillary and 1.56 mm and 2.0 mm for the outer capillary (Fig. 2b). Capillaries were pulled with a micropipette puller (P-1000 and P-97, Sutter Instrument, Novato, CA, USA) and sanded down to the orifice diameter, $D_I = 220$ µm for the inner capillary and $D_O = 200$, 300, and 400 µm for the outer capillary. The tip of the outer capillary was dipped in a silane solution (n-octadecyltrimethoxysilane, Gelest Inc., Morrisville, PA, USA) for several seconds and then dried on air, to get a hydrophobic glass surface.

A gelation bath was placed underneath the capillaries and the falling distance was set at 100 mm. A monochromatic video camera (DMK 33UX273, The Imaging Source Europe GmbH, Bremen, Germany) was used to observe the formation of droplets (Fig. 2c). The diameter of compound droplets, $\widetilde{d}_O$ was calculated based on the droplet generation frequency f, measured from the recorded videos and the total volumetric flowrate:

$$\widetilde{d}_O = \left(\frac{6Q_T}{\pi f}\right)^{1/3} \quad (1)$$

All droplets were gelled for 60 min in a gelation bath containing 0.34 M $CaCl_2$ before further evaluation. Gelled particles were pictured with a single-lens reflex camera (EOS 700D, Canon Inc., Tokyo, Japan) while floating on the surface of the gelation solution. The pictures were used to determine the particle diameters using GNU Image Manipulation Program (GIMP 2.10.36). The diameter of the entire capsule d_O and the core diameter d_I (Fig. 2a) served for the filling degree calculations, assuming a perfect spherical shape of the particles. Particle samples with a coefficient of variation (CV) smaller than 5 % were considered monodisperse [29,30]. At least 10–30 particles were evaluated in each sample. Several process and formulation parameters were varied including Q_T, D_O, Q_I/Q_O, and C_{ALG} (Table S1). The experiments can be divided in three parts: maximizing the throughput, maximizing the filling degree of capsules, and optimising the alginate concentration.

To produce one-phase alginate beads for the shrinking study, an adapted microfluidic set-up was used consisting of one inlet Teflon tube and a single capillary (ID/OD = 1.56/2.0 mm) with an orifice diameter of 200 µm. The flow rate was 50 ml/h for 1 wt% and 2 wt% alginate solutions and 15 ml/h for 3 wt% alginate solution. Beads were gelled and stored in 0.34 M $CaCl_2$ solution at room temperature. Pictures of the beads were taken 60 min, 1 day, and 7 days after the gelation has started. The Feret diameters of 15 particles of each sample were measured and used to calculate the mean diameter and the volume of the beads.

3. Results and discussion

3.1. Millifluidic production of uniformly sized spherical core-shell capsules

Fig. 3a shows the formation of a core-shell droplet at the tip of the outer capillary in dripping regime. The droplets are formed at regular time intervals at steady state, which was established ~30 s after the pumps were turned on. The inner jet was formed upstream of the outer capillary tip (Fig. 2c) which allowed self-alignment of inner jet due to focusing effect in the tapered section of outer capillary. It also led to

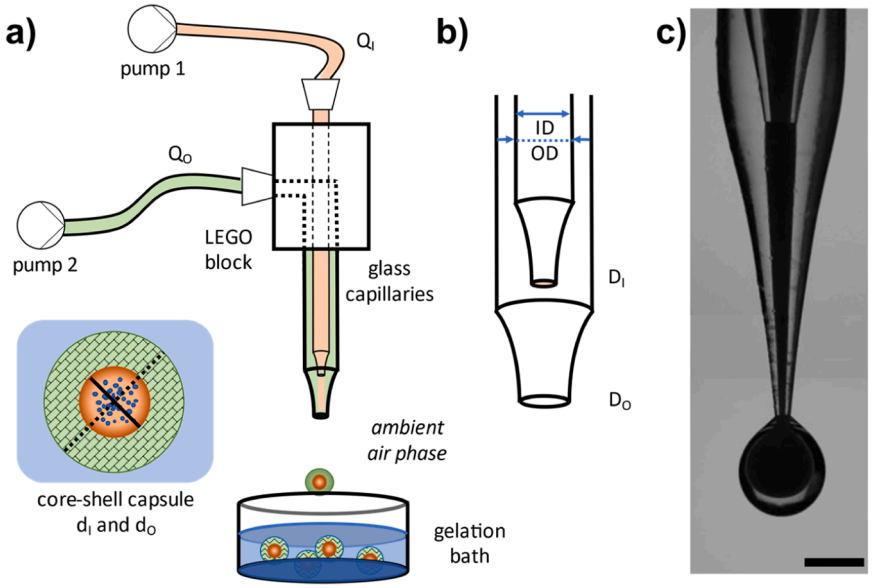

Fig. 2. Production of core-shell capsules using coaxial capillaries aligned by a Lego-inspired micro-machined holder: a) Experimental set-up with syringe pumps, Teflon tubes, Lego block, capillaries, and the gelation bath. The inner and outer volume flowrates are Q_I and Q_O. The produced core-shell capsules consist of a gelled alginate shell (green) and a liquid water-in-oil emulsion core (blue and orange). The inner capsule diameter d_I is shown by solid line and the outer diameter d_O by dashed line; b) Coaxial capillaries with diameters *ID* and *OD* and their orifice diameters D_I and D_O; c) Formation of compound droplet at the tip of the outer capillary. The inner jet was formed upstream of the exit section of the outer capillary. Scale bar: 1 mm.

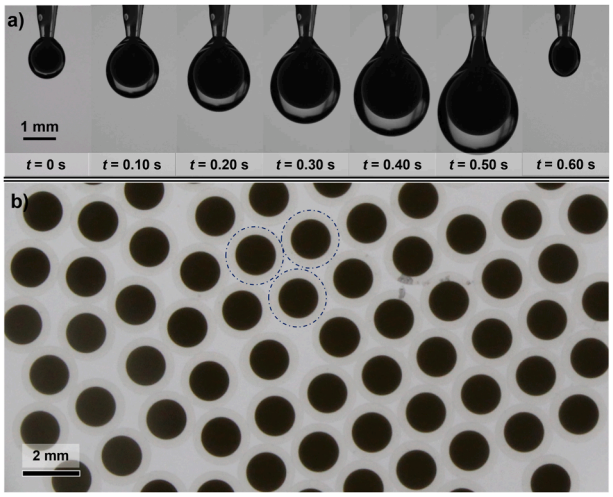

Fig. 3. Production of large, uniform core-shell capsules: a) Time-lapse images showing the formation of core-shell droplets at the tip of the outer capillary at $Q_T = 40$ ml/h, $Q_I/Q_O = 1/4$, $D_O = 300$ µm, $C_{ALG} = 2$ wt%; b) Capsules consisting of a liquid w/o emulsion core and a gelled alginate shell after storage for 1 h in the gelation bath. The outer boundary of several alginate shells is shown by a dash-dotted circle for better visibility.

smaller shear stresses at the inner interface during droplet formation. The dripping process was highly stable over time with ~1.6 droplets per second under the investigated conditions. The diameters of inner and outer droplets were 1.4 mm and 2.4 mm, respectively. Droplets had a rounded form but slightly elongated due to gravitational forces exerting a downward force on the emerging droplet. The pinch-off point was $\sim 9D_O$ downstream of the exit section of the outer capillary. In the supporting information, the videos S1 and S2 are giving an impression of the droplet break-up at different volume flows.

Supplementary material related to this article can be found online at doi:10.1016/j.colsurfa.2025.136541.

In the absence of inertial effects, the outer diameter of compound droplets, once they regain a spherical shape after pinch-off, can be predicted by equating surface tension forces to gravity forces at the breakup point:

$$\tilde{d}_O = \left(\frac{6F_{HB}D_O\gamma}{g\rho^*}\right)^{1/3} \quad (2)$$

where D_O is the orifice diameter of outer capillary, γ the surface tension of alginate solution, F_{HB} the Harkins-Brown correction factor, and ρ^* the density of compound droplets (= 0.988 g/cm^3), calculated based on the volume fraction of alginate solution ($\varphi_{ALG} = Q_O/Q_T$) and the densities of w/o emulsion ($\rho_E = 0.94$ g/cm^3) and alginate solution ($\rho_{ALG} \approx 1$ g/cm^3):

$$\rho^* = \varphi_{ALG}\rho_{ALG} + (1-\varphi_{ALG})\rho_E \quad (3)$$

Since the orifice wall is wetted by the jet (Fig. 3a), the outer tip diameter must be used in (1). The Harkins-Brown correction factor depends on R_O/a [31], where R_O is the orifice radius and a is the capillary length given by: $a = \sqrt{2\gamma/(\rho^* g)}$. Here, $a = 3$ mm and $R_O/a < 1$, which means that $F_{HB} \approx 1$ [31]. From (1), $\tilde{d}_O = 2.2$ mm, which is less than 10 % smaller than the actual diameter of compound droplets. Therefore, for the droplet breakup process shown in Fig. 3(a), the droplet size was only slightly affected by inertial forces. To compare the inertial forces to surface tension, the Weber number of compound jet, *We* can be calculated:

$$We = \frac{\rho^* R_O v^2}{\gamma} = \frac{\rho^* D_O v^2}{2\gamma} \quad (4)$$

where v the average velocity of compound jet at the orifice. Using Eq. (3), the *We* value of 0.08 was calculated. Inertial forces can be neglected for $We \ll 1$, which confirms that the droplet size can be well predicted using (1). The dripping-jetting transition occurs at the critical Weber number (We_{cr}), which is typically between 0.1 and 1 in co-flow microfluidic devices at low capillary numbers of the continuous phase [32].

Fig. 3b shows alginate capsules after the gelation step in the $CaCl_2$ bath. All w/o emulsion drops are encapsulated within the shells indicating that the encapsulation efficiency was ~100 %. Due to small

refractive index difference between $CaCl_2$ solution and alginate gel, the shells are hardly visible in Fig. 3b. For better visibility, several shells are encircled with a dashed line. The capsules have a medium outer diameter d_O of 2.10 mm with a *CV* of 1.9 %, and a medium inner diameter d_I of 1.46 mm with a *CV* of 1.2 %. The shell gelation was triggered by the diffusion of calcium ions from the bath and their binding to carboxylate groups of alginate chains. Due to the bridging of alginate chains by Ca^{2+} ions, the distance between the polymer chains was reduced and a significant fraction of water was expelled from the growing hydrogel network. As a result, the outer shell diameter shrank from 2.4 mm to 2.1 mm upon gelation. The gelled capsules exhibited a regular spherical shape with an average shell thickness of 320 ± 30 μm. Upon impact on the liquid surface, the droplets elongate in the horizontal direction like a pancake (since their kinetic energy is transformed into interfacial energy [33]), but then start to relax toward a spherical shape. If the gelation is faster than the relaxation process, the bending stiffness of the hydrogel shell will eventually balance the surface stresses, which will stop further retraction of the interface and arrest the relaxation process. In this case, the relaxation time was shorter than the gelation time and the droplets regained spherical shape before the shell became too rigid. The gelation time was not determined in this study, but in comparison with other works [34] an alginate layer of 0.3 mm thickness can be estimated to be fully gelled within 3–10 s. The relaxation time of alginate beads without inner core is examined in a detailed study by Godefroid et al. [33]. It is to be expected, however, that the additional oil-water interface between the core and the shell adds a significant force to the relaxation, since the interfacial tension between water and oil is an additional driving force to the gelled layer. This could be the explanation for the high sphericity of the resulting capsules, but remains to be the topic of further studies.

3.2. Influence of total flow rate Q_T on the production of capsules

The results reported in the previous section indicate that the developed co-extrusion process can achieve relatively large and uniform alginate core-shell capsules in dripping regime. However, the size and uniformity of extruded compound droplets are significantly affected by fluid flow rates [22,23,35]. In Fig. S1, the influence of total flow rate Q_T on the shape of compound jet shortly before breakup is shown for three different orifice diameters, D_0 (200, 300, and 400 μm).

In Fig. S1(b), Q_T was gradually increased from 30 ml/h to 100 ml/h at D_0 = 300 μm. The compound jet starts to pinch-off due to increasing gravity force, which is proportional to the droplet volume, pulling the jet downwards and resulting in the appearance of a neck between the jet and the growing droplet. The breakup length (l_b) is the distance between the exit section of the outer capillary and the pinch-off point. At Q_T = 30 ml/h and *We* = 0.04, the breakup length was: $L_b \approx 6.60D_0$ or 1.98 mm. At Q_T = 40 ml/h (*We* = 0.08), $L_b > 9.1D_0$, while at Q_T = 50 ml/h (*We* = 0.12), the pinch-off point was outside the field of view of the used camera system ($L_b > 14D_0$). It means that the breakup length increases with an increase in Q_T, as predicted from the scaling low for a falling viscous jet [21]:

$$L_b \sim \left(\frac{gQ_T^2\mu^4}{\gamma^4}\right)^{1/3} \quad (5)$$

where μ is the effective viscosity of compound jet. Indeed, thinning of the neck is opposed by the influx of liquids into the neck from the incoming co-flow streams, which moves the pinch-off point farther downstream and delays the pinch-off event. At Q_T = 70–100 ml/h (*We* = 0.24–0.50), inertial forces in the jet were so high that the necking occurred significantly below the camera field of view. The width of the compound jet exiting the outer capillary expanded from 300 to 400 μm since to capillary was wetted by the liquids and then expanded again from 400 to 520 μm as the jet moved away from the orifice and evolved from a confined stream into a free jet. At high flow rates, the width of compound jet was only slightly affected by Q_T and mainly depended on D_O.

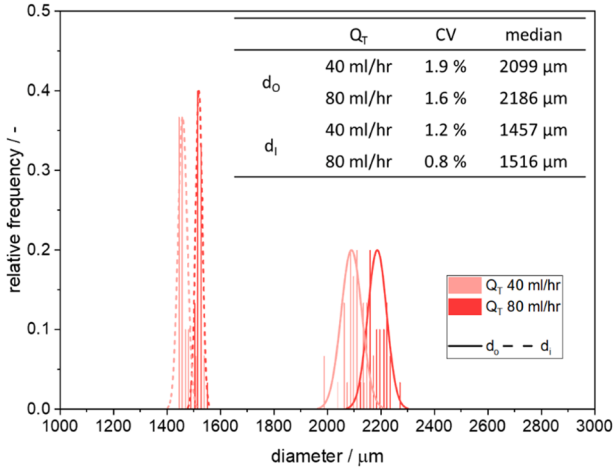

Fig. 4. Particle size distribution of inner diameter d_I and outer diameter d_O of core-shell capsules generated at Q_T = 40 and 80 ml/h after gelation step for 1 h in 0.34 M $CaCl_2$. The coefficients of variation and the median diameters are also displayed. For each sample, 30 capsules were measured, Q_I/Q_O = 1/4, D_O = 300 μm, C_{ALG} = 2 wt%.

Fig. 4 shows the particle size distribution histograms of two samples of core-shell capsules produced at Q_T = 40 and 80 ml/h. Interestingly, capsules produced at the higher flowrate (*We* = 0.64, $L_b/D_0 > 14$) still exhibit a highly monodisperse size distribution with a *CV* of d_0 and d_i values of 1.6 % and 0.8 %, respectively. The outer capsule diameter (d_0) increased only slightly from 2100 μm to 2190 μm in the given range of flow rates. The d_0 values at Q_T = 30 ml/h and 100 ml/h of 1990 ± 21 μm and 2230 ± 16 μm, respectively confirm the trend of higher capsule sizes at higher Q_T values. The droplet production in the jetting regime leads to smaller droplet sizes compared to those in the dripping regime and an increase of polydispersity [22]. The displayed results, however, indicate that capsules are still formed in a dripping-like manner at Q_T = 80 and 100 ml/h. The increased particle size at higher flow rates can be explained by fluid influx into the growing droplet during the necking phase. An increase of the flowrate leads to a faster filling of the drop according to the equation:

$$V_2 = V_1 + Q_T t_{neck} \quad (6)$$

where V_1 and V_2 are the droplet volume at the beginning and the end of the necking process and t_{neck} is the necking time, which depends on the initial jet diameter and the neck thinning rate. For small t_{neck} values (low viscosity fluids), Q_T has a limited impact on droplet size, but for highly viscous liquids, slow jet thinning process (high t_{neck} values) impedes the drop detachment [26].

The effect of Q_T on dripping dynamics at 40 and 80 ml/h is shown in Fig. S2. At Q_T = 80 ml/h, inertial forces dominate the surface tension resulting in a long jet at t = 0.27 s. After the drop is released from the jet, the portion of the liquid upstream of the pinch-off point quickly retreats to the capillary tip under the strong pull of surface tension forces and a new droplet emerges at t = 0.33 s. At Q_T = 40 ml/h, the droplet is formed very close to the capillary tip.

Therefore, a precise detection of the dripping-to-jetting transition at $Q_T > 40$ ml/h was not possible with the used imaging system. Although pictures shown in Fig. S1 imply that the droplets were formed in jetting regime at the applied flowrates, corresponding capsule sizes do not confirm this conclusion. With increasing the filament length, the interfacial tension forces become stronger, which finally lead to the jet breakup [36,37]. Interestingly, inner jet was highly stable resulting in the generation of core-shell droplets, as opposed to double emulsion droplets with multiple cores, which are formed if the inner interface is unstable and rupture significantly before the outer interface. A high

stability of inner jet can be explained by high viscosities of both phases. After injection from the inner capillary, the inner phase flows at the higher velocity than the outer phase. However, the difference in velocities is smaller when the two streams exit the outer capillary due to friction between the two streams in the outer capillary.

3.3. Influence of orifice size of outer capillary D_O on the production of capsules

If the vertical distance between the capillary tips is large enough, the orifice size of inner capillary D_i has a negligible impact on the size of compound droplets and even the size of inner droplets. In that case, the velocity gradient between the inner and outer phase in the compound jet exiting the outer capillary is negligible and the width of inner jet at the exit of the outer capillary depends only on D_O, Q_T, and Q_I/Q_T. Namely, at smaller D_i values, the inner phase will be injected from the inner capillary at higher speed and will face higher deceleration in contact with the outer phase. As a result, the width of inner jet exiting the outer capillary will be the same as at higher D_i values, when the inner stream will be injected at smaller speed but will expand less due to smaller deceleration. Consequently, only the impact of orifice diameter of outer capillary (D_o) on droplet size will be discussed.

In Fig. 5, the capsule diameter (d_o) was plotted against the total flow rate at three different D_o values. The data shows that the capsule diameter increases with the orifice diameter (D_o), as described by Tate's law, (1) [25,31]. The same trend was observed previously for the production of single-phase alginate beads [27,38]. It is commonly explained by an increase of the surface tension force, which affects droplet formation at small values of the Bond number, *Bo* (typically less than one):

$$Bo = \frac{\rho^* g R_O^2}{\gamma} = \frac{\rho^* g D_O^2}{4\gamma} \tag{7}$$

Here, *Bo* is 5.3×10^{-4} for $D_o = 200$ µm and 2.1×10^{-3} for $D_o = 400$ µm, signifying that surface tension effects play an important role. The Tate's law suggests that $d_O \propto D_o^{1/3}$, which is in a good correlation with the experimental data at $Q_T = 40$ and 60 ml/h, with $R^2 = 0.94$ and $R^2 = 0.93$, respectively. In addition, at constant total flow rate, the breakup length is larger at smaller D_o value due to more dominant inertial forces, since $We \propto D_o^{-3}$ at constant Q_T. In Fig. S1, it was shown by comparing L_b values for three different orifice sizes at $Q_T = 40$ ml/h. In addition, the critical flow rate, marked by stars (★), at which the pinch-off point moved outside the viewable area that can be imaged by the camera increased from 40 to 50–80 ml/h, when D_o increased from 200 to 300–400 µm, respectively.

The data in Fig. 5 confirm the previously observed trend of increased capsule sizes at higher Q_T values for a constant orifice size and indicate that the dripping regime can be extended towards higher flowrates by increasing the orifice size. For example, the dripping regime was extended from 70 ml/h at $D_o = 200$ µm to 100 ml/h at $D_o = 300$ µm. The flow rate in dripping regime reached 160 ml/h at $D_o = 400$ µm. All samples were monodispersed with $CV < 5$ % based on 10 evaluated capsules per sample. Therefore, no significant changes in particle size uniformity were found in the investigated range of $0.01 < We < 0.82$, although the total throughput of the device was raised to 160 ml/h. Furthermore, the encapsulation efficiency, defined as the percentage of emulsion cores successfully encapsulated within alginate shells, was higher than 90 % in all experiments, and 100 % in most of them (no single broken capsule was observed). As a conclusion, the process produced monodisperse core-shell capsules of defined size in the range of 1700–2400 µm. It should be noted that d_o was 1700–1900 µm for $D_o = 200$ µm, 2000–2200 µm for $D_o = 300$ µm, and 2200–2400 µm for $D_o = 400$ µm.

3.4. Influence of sodium alginate concentration on the production of capsules

Various studies have shown that the concentration of sodium alginate C_{ALG} in a pre-crosslinked solution has a major impact on the shape and size of resulting alginate beads [27,38,39]. Thus, a comparable influence of C_{ALG} on the morphology of core-shell capsules can be expected. As shown in Table 1, C_{ALG} affects the viscosity and surface tension of the solution and both parameters play important roles in the droplet formation process, as indicated by their influence on *We* and *Oh*. The Ohnesorge number, *Oh* compares viscous forces with inertial and surface tension forces [40,41]:

$$Oh = \frac{\mu}{\sqrt{\rho^* \gamma R_O}} \tag{8}$$

For $Oh \ll 1$, the impact of viscous forces can be neglected and the critical Weber number for the transition from dripping to jetting does not depend on viscosity [42].

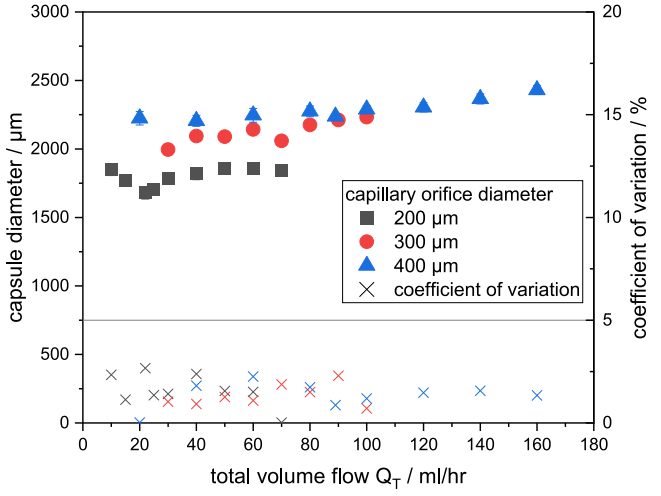

Fig. 5. Influence of the orifice size of outer capillary on the size of core-shell capsules and the corresponding coefficient of variation at different total flow rates. Capsules were gelled for 60 min in 0.34 M $CaCl_2$ solution before observation. For each data point, 10 capsules were measured. Other conditions: $Q_I/Q_O = 1/4$, $C_{ALG} = 2$ wt%.

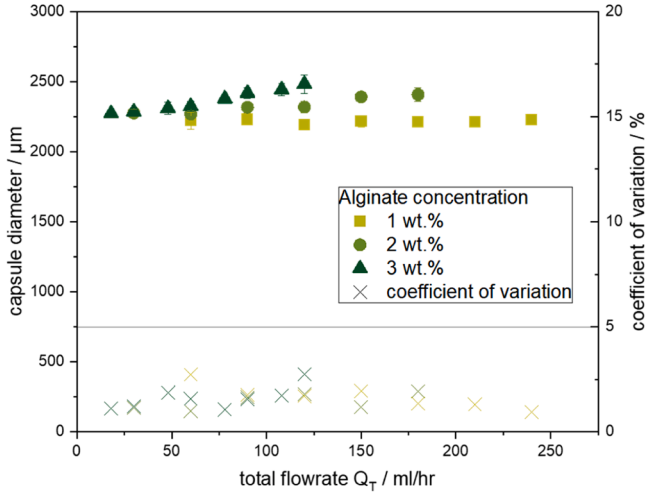

Fig. 6. Influence of the alginate concentration in the outer phase of a compound jet on the size of core-shell capsules and the corresponding coefficient of variation at different total flow rates. Capsules were gelled for 60 min in 0.34 M $CaCl_2$ solution before observation. For each data point, 10 capsules were measured. Other conditions: $Q_I/Q_O = 1/5$, $D_O = 400$ µm.

In Fig. 6, the size of capsules produced in dripping mode using 1 wt%, 2 wt% and 3 wt% alginate solution was plotted against the total flow rate for $Q_I/Q_O = 1/5$ and $D_O = 400$ µm. The *Oh* number was roughly 1, 10, and 50 for $C_{ALG} = 1$, 2, and 3 wt%, respectively. Since $Oh \geq 1$ in these experiments, the critical Weber number We_{crit} for the transition from dripping to jetting is a function of *Oh*. It is known from previous studies on the breakup of one-phase jets that higher *Oh* values lead to smaller We_{crit} values; thus jetting occurs at lower flowrates for higher *Oh* numbers [43]. It is because the time scale for jet breakup depends on the *Oh* value: the breakup time is $t_\nu \equiv \mu R_O/\gamma$ for $Oh \gg 1$, and $t_\mu \equiv \mu^3/(\rho^*\gamma^2)$ for $Oh \sim 1$ [43]. In both cases, the time scale for the flow is $t_f \equiv R_O/u$. The transition to jetting occurs when the jet flow time reaches the breakup time. When $Oh \gg 1$, the transition to jetting occurs at $t_f = t_\nu$ and hence $u_{crit} \propto \gamma/\mu$, where u_{crit} is the critical velocity for the dripping-jetting transition. On the other hand, when $Oh \sim 1$, jetting occurs when $t_f = t_\mu$ and hence $u_{crit} \propto R_O\rho^*\gamma^2/\mu^3$. In both cases, a lower viscosity (concentration) of alginate solution should enable higher flowrates in dripping regime. The same conclusion follows from the results in Fig. 6, since the dripping-to-jetting transition occurred at $Q_T = 120$ ml/h for $C_{ALG} = 3$ wt% and 240 ml/h at $C_{ALG} = 1$ wt%. The critical Weber number was 1.06 at $C_{ALG} = 3$ wt% and much smaller at smaller values of the Ohnesorge number.

Also, higher alginate concentrations led to larger capsules since the breakup time was longer allowing more liquid to flow into the growing droplet during necking phase. At a constant volume flowrate of 120 ml/h, the diameter of the capsules increased from 2190 µm to 2320 µm and 2480 µm due to increase in C_{ALG} from 1 wt% to 2 wt% and 3 wt% respectively. The same effect was observed at lower flowrates of 90 ml/h and 60 ml/h, although the effect was less pronounced, as predicted by Eq. (5). The same trend was observed for the production of single-phase alginate beads using different dripping methods with larger beads produced at higher alginate concentrations [26,38]. The alginate concentration affects not just the capsule size, but also the jet breakup length, L_b. It was shown in Fig. S3 by comparing breakup lengths at $Q_T = 60$ ml/h for three different alginate concentrations. The breakup length was higher at higher jet viscosities, which agrees with Eq. (4). Since the jet breakup time was extended, additional material was delivered though the created neck and larger capsules were formed.

For simple dripping process at $We \ll 1$ when the droplet size is governed by the Bond number, *Bo*, an increase of the alginate concentration leads to smaller droplets, as the surface tension force is reduced. However, it did not result in a smaller capsule size after gelation (Fig. 6), because the decrease in droplet size was offset by smaller shrinkage of more concentrated alginate solutions during gelation. The effect of alginate concentration on the gel shrinkage will be discussed in the next section.

3.5. Gelation of simple droplets of alginate solution

It is widely known that alginate hydrogels shrink during the gel network formation and the degree of syneresis depends on various factors, like the osmolality and pH of the surrounding liquid [44–46]. Since the core volume may also change during gelation due to leakage or swelling effects, in this part of the study the shrinkage was investigated using unfilled alginate beads prepared by extruding pure alginate solution through a single capillary. Fig. 7 displays the shrinkage of alginate droplets in a $CaCl_2$ solution for different initial alginate concentrations. The particle volume is normalized based on the droplet volume before entering the gelation bath, since the alginate concentration affects the droplet generation process, and the initial droplet size was different for different alginate concentrations. All hydrogel beads shrank mainly within the first 60 min ($t = 0$ d) of gelation, reaching between 81 % and 88 % of their total volume reduction reached after 7 days. Therefore, the gelation time of 60 min was used as a standard for all experiments performed in this work.

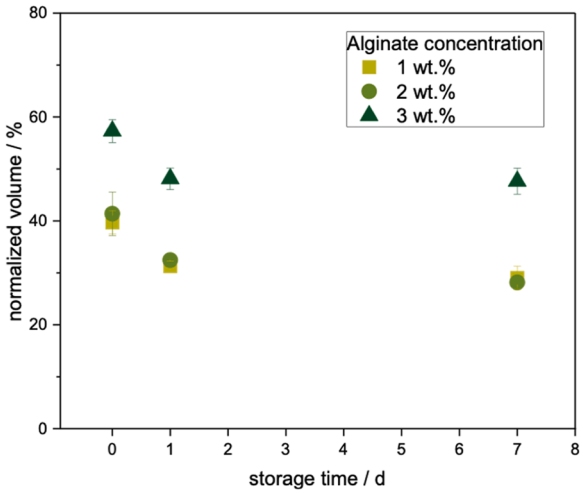

Fig. 7. Shrinkage of alginate beads during storage in 0.34 M $CaCl_2$ solution. The beads were prepared using alginate solutions of different concentrations. The volumes of gel beads were normalized based on drop volumes before gelation. Each data point is an average normalised volume of 15 beads and error bars indicate the standard deviation. The measurements at day 0 were taken after 60 min of gelation.

To quantify the observed volume reductions, the shrinkage factor, *k* was calculated according to Eq. (8):

$$k = \widetilde{V}_O/V_O \tag{9}$$

where $\widetilde{V}_O$ is the droplet volume before gelation and V_O is the bead volume after 60 min of gelation. The *k* values for the solutions containing 1, 2, and 3 wt% alginate, gellified in 0.34 M $CaCl_2$, were 2.517, 2.416, and 1.745, respectively. These values correspond to the alginate concentration in the gel of 2.5 wt%, 4.8 wt% and 5.2 wt%.

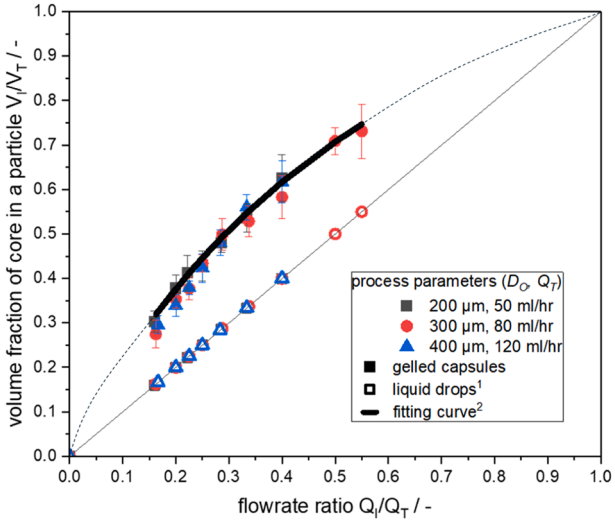

Fig. 8. The filling degree of capsules, expressed as a volume fraction of core, plotted against the flow rate ratio. Formulation: shell = 2 wt% alginate solution, core = 30 wt% w/o emulsion. Shells were gelled in 0.34 M $CaCl_2$ for 60 min. Error bars give the standard deviations for 10 evaluated capsules. The thick solid line is drawn through experimental data points using Eq. (12) with k = 2.416. The dashed line follows Eq. (12) in the entire range of flow rate ratios between 0 and 1. [1]Empty symbols are the data points for liquid capsules. [2]Filled symbols are the experimental data points for solid capsules after gelation.

3.6. Controlling the filling degree of core-shell capsules

The loading capacity or filling degree of capsules is one of the key product parameters and will be defined as a volume fraction of inner phase in capsules (V_I/V_T) after 1 h of gelation, where V_I is the volume of inner phase in a capsule and V_T is the total capsule volume. In Fig. 8, the filling degrees of capsules produced using different orifice sizes are plotted as a function of Q_I/Q_T for the alginate concentration of 2 wt%. At each orifice size D_O, the flow rates Q_I and Q_O have been varied in different ratios at constant total flow rate to change the flow rate ratio Q_I/Q_T. The experimental conditions in these experiments are shown in Table S1. The total flow rates were selected based on previous experiments to maximise the throughput and achieve a stable droplet generation in dripping regime. For making capsules with high encapsulation efficiency, the maximum Q_I/Q_O ratio was 1/1.5 ($Q_I/Q_T = 0.4$) for $D_O = 200$ μm and $D_O = 400$ μm, while the maximum Q_I/Q_O value was 1/0.8 ($Q_I/Q_T \approx 0.55$) for $D_O = 300$ μm. Higher Q_I/Q_T values led to wetting problems and unstable droplet formation. Additionally, liquid shells were too thin and prone to breakage when hitting the gelation bath surface.

The mass balance equations for the droplet formation process can be written as follows:

$$Q_I = \widetilde{V}_I f \tag{10}$$

$$Q_T = \widetilde{V}_T f \tag{11}$$

where f is the frequency of droplet generation and $\widetilde{V}_I$, $\widetilde{V}_O$, and $\widetilde{V}_T$ are the inner phase volume, the outer phase volume and the total volume of core/shell droplets before gelation. Therefore, $Q_I/Q_T = \widetilde{V}_I/\widetilde{V}_T$, which means that the filling degree of liquid capsules is equal to the flow rate ratio, Q_I/Q_T, and the corresponding data points for liquid capsules lie on the diagonal line in Fig. 8. For capsules with gelled shells, the core volume is: $V_I \approx \widetilde{V}_I$ (assuming no change in core volume during gelation) and the shell volume is: $V_O = \widetilde{V}_O/k$ (from Eq. (8)). Using these assumptions and combining Eqs. (9) and (10) with $V_T = V_I + V_O$, the following equation for the filling degree of gelled capsules can be derived:

$$\frac{V_I}{V_T} = \frac{k\frac{Q_I}{Q_T}}{1 + (k-1)\frac{Q_I}{Q_T}} \tag{12}$$

The resulting curve for $k = 2.416$ (2 wt% alginate and 60 min gelation in 0.34 M $CaCl_2$) is plotted as a dashed line in Fig. 8 and the thick black line is the segment of that curve passing through the experimental data points. The coefficients of determination of the measured V_I/V_T values and the corresponding values calculated by Eq. (12) are $R^2 = 99.9$ %, 97.0 %, and 99.7 %, for the experiments with $D_O = 200$ μm, 300 μm and 400 μm, respectively. The high values of R^2 close to 100 % indicate a good fit of the measured data to the proposed model. Thus, the model assumptions are accurate and the core volume can be assumed as constant during gelation. In addition, the shrinkage rate of alginate solution within core/shell capsules is not affected by the core material.

The results in Fig. 8 lead to several conclusions. First, the volume fraction of core liquid in gelled alginate capsules can be controlled by adjusting the flow rates, Q_I and Q_T. To predict the filling degree of the capsules, shrinkage of alginate solution upon gelation must be considered and can be described by Eq. (8). Secondly, the size of core-shell capsules increases with increasing the flowrate ratio Q_I/Q_T at a constant Q_T value, as the volume fraction of alginate solution in the droplet decreases and smaller contraction of the total volume occurs. For example, the capsule size at $D_O = 300$ μm and $Q_T = 80$ ml/hr increased from $d_O = 2120$ μm at $Q_I/Q_T = 0.16$ to $d_O = 2300$ μm at $Q_I/Q_T = 0.55$. Similar trends were observed in the experiments with other orifice sizes. Thirdly, no significant influence of the orifice size on the loading capacity was observed. This indicates that the process is scalable and promises the potential increase of the total throughput by increasing the orifice sizes without compromising the loading capacity. The highest loading capacity of $V_I/V_T = 73$ % was achieved with $D_O = 300$ μm at the flow rate ratio of $Q_I/Q_T = 0.55$.

3.7. Swelling of inner water droplets in core-shell capsules

During the gelation process or storage for longer time, both regions of the capsule, the emulsion core and the alginate shell, may experience size changes. The changes in the core volume may occur due to shrinkage or swelling of inner water droplets or due to their escape (release) into the gelation bath solution. Concerning the shrinkage and swelling phenomena, they usually take place by molecular diffusion due to the osmotic pressure gradient between the inner water phase and the ambient water phase. The emulsion core of the capsules is in direct contact with the alginate gel, which is a highly porous matrix filled with water and therefore, does not provide a barrier to small water molecules. Consequently, mass transfer of water between the inner and outer aqueous phase is possible [47].

Fig. 9 shows the core volume of different samples of core/shell capsules before and after the gelation process. The capsules were prepared using $D_O = 400$ μm and $Q_T = 120$ ml/h and the gelation process took 60 min. During that period, the core volume increased in a range of 1.5–12 % ($\Delta V_I = 0.027$–0.47 mm^3) indicating the diffusion of water from the outer phases towards the capsule core. A general trend of higher swelling degree at increased filling degrees, thus for larger cores, was observed. Based on the Fick's law, the diffusion rate is proportional to the surface area between two phases [48], but the shell thickness, which is smaller for larger cores, may also play some role. Due to relatively short gelation time of 1 h, it is more likely that the swelling of inner droplets was due to release of water from the shell during cross-linking, rather than due to diffusion of water from the gelation bath. Nevertheless, the maximum core swelling of $\Delta V_I = 0.47$ mm^3 is negligible compared to the shell shrinking of $\Delta V_O = 4.22$ mm^3, which means that most of the water expelled from the shell during gelation was transferred into the gelation bath and only small fraction was transferred inwards. Probably, water removed from the innermost layers of alginate solution diffused into the inner water droplets and this transfer was likely facilitated by surfactant molecules dissolved in the oil phase. The

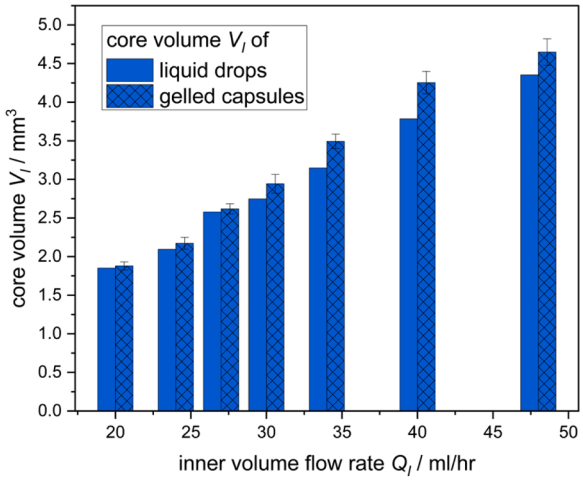

Fig. 9. The core volume in core/shell alginate capsules before and after the shell gelation. The capsules were produced at the total flow rate of $Q_T = 120$ ml/h with an orifice size of $D_O = 400$ μm. Formulation: shell = 2 wt% alginate solution, core = 30 wt% w/o emulsion. Capsules were gelled in 0.34 M $CaCl_2$ for 60 min before the core diameter was measured. The core volume was consequently derived from the diameter, assuming that the core is a sphere. Error bars indicate the standard deviation of 10 evaluated capsules.

observed swelling degrees of the core correspond to the volume increase of inner droplets from 5 % to 40 %. As stated before, core volume changes can be neglected compared to shell volume changes and thus, the model presented by Eq. (12) is in good agreement with the experimental data.

4. Conclusions

The experiments in this study have shown that the developed co-extrusion process could produce stable core-shell milli-capsules composed of a gelled alginate shell and a liquid w/o emulsion core. Droplet formation in a quiescent air led to large, monodisperse, uniform, and spherical capsules. A systematic variation of the process parameters D_O and Q_T revealed their relationship to the capsule parameters d_O and CV. Monodisperse capsule populations with the size ranging from 1700 to 2400 μm were produced using 2 wt% alginate solutions at the total flowrates up to 160 ml/h per capillary. A decrease in the alginate concentration to 1 wt% enabled an increase of the total throughput to 240 ml/h and an increase of the capsule size from up to nearly 2500 μm. Long breakup lengths at increased fluid flow rates suggested that the transition to jetting occurred, but capsule sizes were not significantly affected indicating that the dripping regime was sustained under these flow rates.

Furthermore, the filling degree of capsules was tuned by varying the applied inner and outer volume flowrate. The maximum Q_I/Q_O ratio of 1/0.8 was achieved, before instability issues during the droplet production process led to an increased capsule breakage. A comparison of the corresponding flowrate ratio and the fraction of core material in the capsules revealed the influence of the gelation step on the size of the gelled core-shell capsules. Capsule cores were found to grow during the gelation period depending on the initial core size, suggesting diffusion of water from the outer phases towards the capsule core. Contrary, capsule shells were subjected of shrinkage due to alginate gel formation. The experimental observations were used to define assumptions for a mathematical model which was developed to predict the resulting size of core-shell capsules using an experimentally determined gel shrinkage factor. The final size and loading capacity of core-shell capsules generated using various orifice diameters were predicted with accuracies above $R^2 = 97.0$ %.

The fabricated emulsion-filled alginate capsules with a creamy core and a jelly shell can be used as a model system for a plant-based fish egg alternative (vegan caviar) and can be incorporated into various food products to suppress appetite and increase feelings of satiety and fullness [49]. In addition, developed alginate capsules can be used as organoid biocarriers in tissue regenerative medicine [50], a robust chassis for artificial cells and a portable platform for artificial membrane studies in synthetic biology [51].

CRediT authorship contribution statement

Johannes Marburger: Writing – original draft, Visualization, Methodology, Investigation, Formal analysis. **Nico Leister:** Writing – review & editing, Supervision, Project administration, Methodology, Conceptualization. **Goran T. Vladisavljević:** Writing – review & editing, Methodology, Formal analysis, Conceptualization.

Declaration of Competing Interest

The authors declare the following financial interests/personal relationships which may be considered as potential competing interests: Goran T. Vladisavljevic reports travel was provided by Karlsruhe Institute of Technology. Johannes Marburger reports travel was provided by German Academic Exchange Service. If there are other authors, they declare that they have no known competing financial interests or personal relationships that could have appeared to influence the work reported in this paper.

Acknowledgments

The authors acknowledge the financial support of PROMOS for the travelling and living expenses of Johannes Marburger during his research stay at Loughborough University. The authors also acknowledge the financial support from International Excellence Fellowship of KIT for the research stay of Goran Vladisavljević at Karlsruhe Institute of Technology.

Appendix A. Supporting information

Supplementary data associated with this article can be found in the online version at doi:10.1016/j.colsurfa.2025.136541.

Data availability

Data will be made available on request.

References

[1] C. Bennacef, S. Desobry, L. Probst, S. Desobry-Banon, Alginate based core–shell capsules production through coextrusion methods: recent applications, Foods 12 (2023), https://doi.org/10.3390/foods12091788.
[2] A.S. Ismail, G.R. Goodwin, J.R. Castrejon-Pita, A.J. Noyce, H.S. Azevedo, A novel capsule-based smell test fabricated via coaxial dripping, J. R. Soc. Interface 18 (2021) rsif.2021.0039, 20210039. https://doi.org/10.1098/rsif.2021.0039.
[3] P.J.R. Cohen, E. Luquet, J. Pletenka, A. Leonard, E. Warter, B. Gurchenkov, J. Carrere, C. Rieu, J. Hardouin, F. Moncaubeig, M. Lanero, E. Quelennec, H. Wurtz, E. Jamet, M. Demarco, C. Banal, P.V. Liedekerke, P. Nassoy, M. Feyeux, N. Lefort, K. Alessandri, Engineering 3D micro-compartments for highly efficient and scale-independent expansion of human pluripotent stem cells in bioreactors, Biomaterials 295 (2023) 122033, https://doi.org/10.1016/j.biomaterials.2023.122033.
[4] S.H. Ching, N. Bansal, B. Bhandari, Alginate gel particles–A review of production techniques and physical properties, Crit. Rev. Food Sci. Nutr. 57 (2017) 1133–1152, https://doi.org/10.1080/10408398.2014.965773.
[5] H. Bojorges, A. López-Rubio, A. Martínez-Abad, M.J. Fabra, Overview of alginate extraction processes: impact on alginate molecular structure and techno-functional properties, Trends Food Sci. Technol. 140 (2023) 104142, https://doi.org/10.1016/j.tifs.2023.104142.
[6] E. Martins, D. Poncelet, M. Marquis, J. Davy, D. Renard, Monodisperse core-shell alginate (micro)-capsules with oil core generated from droplets millifluidic, Food Hydrocoll. 63 (2017) 447–456, https://doi.org/10.1016/j.foodhyd.2016.09.018.
[7] A. Schmit, L. Courbin, M. Marquis, D. Renard, P. Panizza, A pendant drop method for the production of calibrated double emulsions and emulsion gels, RSC Adv. 4 (2014) 28504–28510, https://doi.org/10.1039/C4RA02464H.
[8] M. Liu, D. Yin, H. Fu, F. Deng, G. Peng, G. Shu, Z. Yuan, F. Shi, J. Lin, L. Zhao, L. Yin, G. Fan, Double-coated enrofloxacin microparticles with chitosan and alginate: preparation, characterization and taste-masking effect study, Carbohydr. Polym. 170 (2017) 247–253, https://doi.org/10.1016/j.carbpol.2017.04.071.
[9] Y. Gao, X. Li, Y. Xie, X. Huang, C. Cheng, D. Julian McClements, L. Zhang, X. Chen, L. Zou, L. Wei, Encapsulation of bitter peptides in diphasic gel double emulsions: Bitterness masking, sustained release and digestion stability, Food Res. Int. 162 (2022) 112205, https://doi.org/10.1016/j.foodres.2022.112205.
[10] R. Al Nuumani, G.T. Vladisavljević, M. Kasprzak, B. Wolf, In-vitro oral digestion of microfluidically produced monodispersed W/O/W food emulsions loaded with concentrated sucrose solution designed to enhance sweetness perception, J. Food Eng. 267 (2020) 109701, https://doi.org/10.1016/j.jfoodeng.2019.109701.
[11] N. Chiu, A. Tarrega, C. Parmenter, L. Hewson, B. Wolf, I.D. Fisk, Optimisation of octinyl succinic anhydride starch stablised w 1 /o/w 2 emulsions for oral destablisation of encapsulated salt and enhanced saltiness, Food Hydrocoll. 69 (2017) 450–458, https://doi.org/10.1016/j.foodhyd.2017.03.002.
[12] E. Martins, D. Poncelet, R.C. Rodrigues, D. Renard, Oil encapsulation techniques using alginate as encapsulating agent: Applications and drawbacks, J. Microencapsul. 34 (2017) 754–771, https://doi.org/10.1080/02652048.2017.1403495.
[13] N.T.T. Uyen, Z.A.A. Hamid, N.X.T. Tram, N. Ahmad, Fabrication of alginate microspheres for drug delivery: a review, Int. J. Biol. Macromol. 153 (2020) 1035–1046, https://doi.org/10.1016/j.ijbiomac.2019.10.233.
[14] M. Pereda, D. Poncelet, D. Renard, Characterization of core-shell alginate capsules, Food Biophys. 14 (2019) 467–478, https://doi.org/10.1007/s11483-019-09595-x.
[15] B. Lupo, A. Maestro, M. Porras, J.M. Gutiérrez, C. González, Preparation of alginate microspheres by emulsification/internal gelation to encapsulate cocoa polyphenols, Food Hydrocoll. 38 (2014) 56–65, https://doi.org/10.1016/j.foodhyd.2013.11.003.

[16] T. Shao, X. Feng, Y. Jin, Y. Cheng, Controlled production of double emulsions in dual-coaxial capillaries device for millimeter-scale hollow polymer spheres, Chem. Eng. Sci. 104 (2013) 55–63, https://doi.org/10.1016/j.ces.2013.09.001.
[17] G. Muschiolik, E. Dickinson, Double emulsions relevant to food systems: preparation, stability, and applications, Compr. Rev. Food Sci. Food Saf. 16 (2017) 532–555, https://doi.org/10.1111/1541-4337.12261.
[18] G.T. Vladisavljević, N. Khalid, M.A. Neves, T. Kuroiwa, M. Nakajima, K. Uemura, S. Ichikawa, I. Kobayashi, Industrial lab-on-a-chip: design, applications and scale-up for drug discovery and delivery, Des. Prod. Charact. Drug Deliv. Syst. Lab—Chip Technol. 65 (2013) 1626–1663, https://doi.org/10.1016/j.addr.2013.07.017.
[19] N. Leister, G.T. Vladisavljević, H.P. Karbstein, Novel glass capillary microfluidic devices for the flexible and simple production of multi-cored double emulsions, J. Colloid Interface Sci. 611 (2022) 451–461, https://doi.org/10.1016/j.jcis.2021.12.094.
[20] L. Yu, Q. Sun, Y. Hui, A. Seth, N. Petrovsky, C.-X. Zhao, Microfluidic formation of core-shell alginate microparticles for protein encapsulation and controlled release, J. Colloid Interface Sci. 539 (2019) 497–503, https://doi.org/10.1016/j.jcis.2018.12.075.
[21] A.S. Chaurasia, S. Sajjadi, Millimetric core–shell drops via buoyancy assisted non-confined microfluidics, Chem. Eng. Sci. 129 (2015) 260–270, https://doi.org/10.1016/j.ces.2015.02.028.
[22] B. Derby, Inkjet printing of functional and structural materials: fluid property requirements, feature stability, and resolution, Annu. Rev. Mater. Res. 40 (2010) 395–414, https://doi.org/10.1146/annurev-matsci-070909-104502.
[23] H. Moghadam, M. Samimi, A. Samimi, M. Khorram, Electro-spray of high viscous liquids for producing mono-sized spherical alginate beads, Particuology 6 (2008) 271–275, https://doi.org/10.1016/j.partic.2008.04.005.
[24] J.M. Montanero, A.M. Gañán-Calvo, Dripping, jetting and tip streaming, Rep. Prog. Phys. 83 (2020) 097001, https://doi.org/10.1088/1361-6633/aba482.
[25] T. Tate, X.X.X. On, the magnitude of a drop of liquid formed under different circumstances, Lond. Edinb. Dublin Philos. Mag. J. Sci. 27 (1864) 176–180.
[26] T.I. Klokk, J.E. Melvik, Controlling the size of alginate gel beads by use of a high electrostatic potential, J. Microencapsul. 19 (2002) 415–424, https://doi.org/10.1080/02652040210144234.
[27] E.-S. Chan, B.-B. Lee, P. Ravindra, D. Poncelet, Prediction models for shape and size of ca-alginate macrobeads produced through extrusion–dripping method, J. Colloid Interface Sci. 338 (2009) 63–72, https://doi.org/10.1016/j.jcis.2009.05.027.
[28] M.V. Bandulasena, G.T. Vladisavljević, B. Benyahia, Versatile reconfigurable glass capillary microfluidic devices with Lego® inspired blocks for drop generation and micromixing, J. Colloid Interface Sci. 542 (2019) 23–32, https://doi.org/10.1016/j.jcis.2019.01.119.
[29] L. Liu, F. Wu, X.-J. Ju, R. Xie, W. Wang, C.H. Niu, L.-Y. Chu, Preparation of monodisperse calcium alginate microcapsules via internal gelation in microfluidic-generated double emulsions, J. Colloid Interface Sci. 404 (2013) 85–90, https://doi.org/10.1016/j.jcis.2013.04.044.
[30] E.-S. Chan, T.-K. Lim, W.-P. Voo, R. Pogaku, B.T. Tey, Z. Zhang, Effect of formulation of alginate beads on their mechanical behavior and stiffness, Particuology 9 (2011) 228–234, https://doi.org/10.1016/j.partic.2010.12.002.
[31] C. Clanet, J.C. Lasheras, Transition from dripping to jetting, J. Fluid Mech. 383 (1999) 307–326, https://doi.org/10.1017/S0022112098004066.
[32] J.K. Nunes, S.S.H. Tsai, J. Wan, H.A. Stone, Dripping and jetting in microfluidic multiphase flows applied to particle and fibre synthesis, J. Phys. Appl. Phys. 46 (2013) 114002, https://doi.org/10.1088/0022-3727/46/11/114002.
[33] J. Godefroid, D. Bouttes, A. Marcellan, E. Barthel, C. Monteux, Surface stress and shape relaxation of gelling droplets, Soft Matter 19 (2023) 7787–7795, https://doi.org/10.1039/D3SM00533J.
[34] P. Lee, M.A. Rogers, Effect of calcium source and exposure-time on basic caviar spherification using sodium alginate, Int. J. Gastron. Food Sci. 1 (2012) 96–100, https://doi.org/10.1016/j.ijgfs.2013.06.003.
[35] S.-K. Moon, I.W. Cheong, S.-W. Choi, Effect of flow rates of the continuous phase on droplet size in dripping and jetting regimes in a simple fluidic device for coaxial flow, Colloids Surf. Physicochem. Eng. Asp. 454 (2014) 84–88, https://doi.org/10.1016/j.colsurfa.2014.04.006.
[36] T. Glawdel, C. Elbuken, C.L. Ren, Droplet generation in microfluidics, in: D. Li (Ed.), Encycl. Microfluid. Nanofluidics, Springer, US, Boston, MA, 2013, pp. 1–12, https://doi.org/10.1007/978-3-642-27758-0_1713-1.
[37] A.S. Utada, L.Y. Chu, A. Fernandez-Nieves, D.R. Link, C. Holtze, D.A. Weitz, Dripping, jetting, drops, and wetting: the magic of microfluidics, MRS Bull. 32 (2007) 702–708, https://doi.org/10.1557/mrs2007.145.
[38] F. Davarcı, D. Turan, B. Ozcelik, D. Poncelet, The influence of solution viscosities and surface tension on calcium-alginate microbead formation using dripping technique, Food Hydrocoll. 62 (2017) 119–127, https://doi.org/10.1016/j.foodhyd.2016.06.029.
[39] D.B. Seifert, J.A. Phillips, Production of small, monodispersed alginate beads for cell immobilization, Biotechnol. Prog. 13 (1997) 562–568, https://doi.org/10.1021/bp9700723.
[40] W.V. Ohnesorge, Die Bildung von Tropfen an Düsen und die Auflösung flüssiger Strahlen, ZAMM - J. Appl. Math. Mech. Z. F. üR. Angew. Math. Mech. 16 (1936) 355–358, https://doi.org/10.1002/zamm.19360160611.
[41] H.J. Subramani, H.K. Yeoh, R. Suryo, Q. Xu, B. Ambravaneswaran, O.A. Basaran, Simplicity and complexity in a dripping faucet, Phys. Fluids 18 (2006) 032106, https://doi.org/10.1063/1.2185111.
[42] A. Bertrandias, H. Duval, J. Casalinho, M.L. Giorgi, Dripping to jetting transition for cross-flowing liquids, Phys. Fluids 29 (2017) 044102, https://doi.org/10.1063/1.4979266.
[43] B. Ambravaneswaran, H.J. Subramani, S.D. Phillips, O.A. Basaran, Dripping-jetting transitions in a dripping faucet, Phys. Rev. Lett. 93 (2004) 034501, https://doi.org/10.1103/PhysRevLett.93.034501.
[44] N.M. Velings, M.M. Mestdagh, Physico-chemical properties of alginate gel beads, Polym. Gels Netw. 3 (1995) 311–330, https://doi.org/10.1016/0966-7822(94)00043-7.
[45] B.-B. Lee, P. Ravindra, E.-S. Chan, Size and shape of calcium alginate beads produced by extrusion dripping, Chem. Eng. Technol. 36 (2013) 1627–1642, https://doi.org/10.1002/ceat.201300230.
[46] A. Martinsen, G. Skjåk-Bræk, O. Smidsrød, Alginate as immobilization material: I. Correlation between chemical and physical properties of alginate gel beads, Biotechnol. Bioeng. 33 (1989) 79–89, https://doi.org/10.1002/bit.260330111.
[47] N. Leister, H.P. Karbstein, Evaluating the stability of double emulsions—a review of the measurement techniques for the systematic investigation of instability mechanisms, Colloids Interfaces 4 (2020), https://doi.org/10.3390/colloids4010008.
[48] E.L. Cussler, Diffusion: mass transfer in fluid systems, Cambridge University Press, 2009.
[49] M.N. Corstens, F.J. Troost, A.M.E. Alleleyn, T. Klaassen, C.C. Berton-Carabin, K. Schroën, A.A.M. Masclee, Encapsulation of lipids as emulsion-alginate beads reduces food intake: a randomized placebo-controlled cross-over human trial in overweight adults, Nutr. Res. 63 (2019) 86–94, https://doi.org/10.1016/j.nutres.2018.12.004.
[50] F. He, T. Tao, H. Liu, Y. Wang, K. Cui, Y. Guo, J. Qin, Controllable fabrication of composite core–shell capsules at a macroscale as organoid biocarriers, ACS Appl. Biol. Mater. 4 (2021) 1584–1596, https://doi.org/10.1021/acsabm.0c01441.
[51] D.K. Baxani, A.J.L. Morgan, W.D. Jamieson, C.J. Allender, D.A. Barrow, O. K. Castell, Bilayer networks within a hydrogel shell: a robust chassis for artificial cells and a platform for membrane studies, Angew. Chem. Int. Ed. 55 (2016) 14240–14245, https://doi.org/10.1002/anie.201607571.